Applied methodology

A study of lead uptake and distribution in horns from lead-dosed goats using synchrotron radiation-induced micro X-ray fluorescence elemental imaging

Mina W. Tehrani[a,b,1], Rong Huang[c], Diana Guimarães[a,b], Louisa Smieska[c], Arthur Woll[c], Patrick J. Parsons[a,b,2,*]

[a] Laboratory of Inorganic and Nuclear Chemistry, Wadsworth Center, New York State Department of Health, PO Box 509 Albany, NY 12201, USA
[b] Department of Environmental Health Sciences, University at Albany, Albany, NY 12222, USA
[c] Cornell High Energy Synchrotron Source, Ithaca, NY 14850, USA

A B S T R A C T

Objective: The principal goal of this study was to investigate the uptake and distribution of lead (Pb) in the horns of Pb-dosed goats, and to explore possible links to their historical Pb dosing records. Horn is a keratinized material that grows in discrete increments with the potential to preserve the historical record of past environmental exposures. While previous studies have leveraged this potential to examine environmental and biological phenomena in horns, Pb uptake has never been explored.

Methods: Horns were collected *post-mortem* from three goats that had been previously used to produce blood lead reference materials for the New York State proficiency testing program. The animals were periodically dosed with lead acetate, administered orally in a capsule, over a 5 to 8-year period. Horn cross sections were taken from each animal and analyzed using synchrotron radiation-induced micro X-ray fluorescence spectrometry (SR-µXRF) at the Cornell High Energy Synchrotron Source (CHESS).

Results: Elemental distribution maps were obtained by SR-µXRF for Pb, Ca, S, Se, and three other elements (Br, Zn and Cu), with values reported quantitatively as a mass fraction (µg/g for trace elements and mg/g for Ca and S). Accumulations of Pb were clearly visible as a series of narrow "rings" in each of the horn samples analyzed. The elements Ca, S, Br, Zn, and Cu were also detected as discrete rings within each cross-section, with Br strongly correlated with S in the samples examined. A marginal increase in Se may coincide with Pb accumulation in horn cross-sections. Annual mineralization estimates based on the relative distribution of Ca and S were used to establish a tentative timeline for horn growth, with each timeline linked to the pattern of Pb accumulation in the corresponding horn cross-section sample.

Conclusions: Following ingestion, absorbed Pb is eventually deposited into caprine horns, resulting in discrete accumulations or "rings." Elemental mapping by SR-µXRF clearly show Ca-rich layers that vary with annual periodicity, consistent with previous reports of horn mineralization. Localized enrichment of Cu, Zn, Br and S appear to coincide with the keratinized regions related to the annual growth ring pattern in horns. Spatial analysis of horns for Pb accumulation may be useful as a qualitative marker of time-resolved exposures that may reflect specific periods of acute Pb absorption.

1. Introduction

Hard keratinized materials are a diverse family of tissues that includes horns, nails, hair, hooves, tortoiseshell scutes, and others, with functions ranging from thermal regulation to self-defense. Enrichment of the disulfide-bonded amino acid cysteine (cystine) gives these tissues their characteristic toughness. Free cysteine also binds to some metal ions with high affinity, and it has been shown that keratinized tissues can bio-concentrate toxic trace elements such as mercury and arsenic [1]. Horns and other hard keratinized tissues grow incrementally, forming metabolically inert layers that can preserve historical elemental exposure information over time [2]. Other materials that grow

---

in increments and can be used to study historical events include otoliths, teeth, mollusk shells, corals, and trees, among other animal and plant tissues [2–4]. To our knowledge, only one other study has used animal horns to reconstruct past exposures and environmental events based on trace element analysis. Caumette et al. reported on the uptake and spatial distribution of arsenic (As) and iodine (I) in the horns of seaweed-eating wild sheep from North Ronaldsay, Scotland, using the sheep horns as "archives" of the sheep's exposure to those elements [5]. Several studies have used the isotopic carbon and nitrogen data from horns to investigate (a) animal diets and habitats [6,7], (b) climatic changes [8], and (c) to validate radiocarbon dating methodology [9].

Lead (Pb) is a ubiquitous environmental contaminant with a wide range of adverse health effects in humans and animals. Because of the persistence of Pb in the environment and its long residence time in the body, the Pb burden in the human body and in ecosystems may reflect past as well as recent exposures. Historical Pb emissions have been investigated using corals [10], otoliths [11], trees [12], sediment cores [13], and snail shells [14], among other sample matrices. Past Pb exposures in humans have been studied mainly using bone Pb measurements, while keratinized tissues (hair and nails) are less common [15].

Due to the challenge of exogenous contamination in many keratinized tissues, few studies have been able to demonstrate an association between Pb exposure and Pb content. Some have reported that Pb in hair and/or nails is an unreliable biomarker of Pb exposure [16–18]. Contamination notwithstanding, the excretion of Pb in human hair has been demonstrated to some extent in at least two previous studies [19,20]. While horn is also a keratinized tissue, it has a relatively low surface area-to-volume ratio, and therefore reduced exogenous Pb deposition.

In this study, we report on the uptake and spatial distribution of Pb, along with other detectable elements, in the horns of adult goats that had been periodically dosed with Pb over a period of 5 to 8 years. These lead-dosed goats were used as a source of blood pools containing physiologically-bound Pb, which is important for producing matrix-based reference materials for validating analytical blood Pb measurements [21]. Previous studies from our laboratory have reported on caprine blood Pb reference pools produced from these goats [21,22], and on the uptake and accumulation of Pb in caprine long bones [23], brain [24], and other soft tissues [25]. The principal aim of this study is to explore the relationship between the Pb dosing history and spatial distributions of Pb in horns from this same population of goats. Synchrotron radiation-based micro X-ray fluorescence (SR-μXRF) was used to create elemental maps of several horn cross sections to provide new information on the relationship between Pb dose and Pb excretion, as well as on the distribution of the elements Ca, S, Se, Zn, Cu, and Br in caprine horns.

2. Materials and methods

2.1. Sources of horns

Horns were collected *post-mortem* from three male animals selected from a herd of goats maintained by the New York State Department of Health's (NYS DOH) Wadsworth Center, as described elsewhere [22,26]. Over the last three decades, more than 60 goats have been dosed periodically with Pb to produce Pb-enriched blood reference pools for distribution in the NYS DOH's blood Pb proficiency testing (PT) program. None of the goats are offspring of other dosed goats in the program, making substantial *in utero* Pb exposure unlikely. Animal use protocols were reviewed and approved by the Wadsworth Center Institutional Animal Care and Use Committee (IACUC protocol #16-096); the Wadsworth Center is accredited by the Association for Assessment and Accreditation of Laboratory Animal Care. Adult goats were dosed with Pb, as Pb acetate, in oral gelatin capsules over several multi-day events, before blood was collected for PT pools. At the end of their working lives, these animals were euthanized on the advice of the

attending veterinarian responsible for the program. Necropsies were performed in which the major organs and tissues including the liver, kidneys, heart, lungs, horns, and long bones were harvested for research purposes. Horns were collected as convenience samples from approximately 20 animals and archived for research studies. Horn samples used in this study were derived from animals identified by *year of animal birth – number* as 1982-5, 2001-5, and 2002-1. All three animals were first dosed at 4 years of age. Goat 2001-5 was born on April 5, 2001 and died on October 3, 2016 (age at death 15 years and 6 months). Goat 2002-1 was born on March 4, 2002 and died on January 28, 2015 (age at death 12 years and 10 months). Goat 1982-5 was born in 1982 and died in 1994; exact birth, death and dosing dates are not known. The full dosing history for goats 2001-5 and 2002-1, including information on daily dosing and multi-day dose events, are shown in the Supplementary Table.

2.2. Sample preparation for SR-μXRF imaging

Entire horns, ranging in length from ˜20 to 50 cm, were removed proximal to the deceased animal's skull using a Stryker autopsy saw (Kalamazoo, MI). Horns were washed with de-ionized water to remove adhering hair, blood, and other debris to reduce contamination of samples. Transverse sections were cut using a diamond-disk blade attached to a Dremel tool (Racine, WI) by making two cuts near the tip of each horn, where the most rings are present (Fig. 1). The two cuts were approximately 0.5 cm apart to create as thin a section as possible while maintaining sample integrity. Transverse sections were then ground to a thickness of between 230 and 430 μm using a Buehler grinder polisher (Lake Bluff, Illinois) with 800 and 600-grit polishing papers, respectively. Polishing also served the purposes of removing surface contamination and smoothing the sample surface. Samples were mounted for SR-μXRF analysis by adhesion to DuPont Kapton® tape (Wilmington, DE) on the back side. The surface to be analyzed was left uncovered.

Three horn cross sections from the three different animals were analyzed by SR-μXRF. The three samples are identified by *s+ goat identifier* as s2001-5, s1982-5, and s2002-1. For quality control (QC) purposes, pellets were prepared from two certified reference materials (CRMs) based on hair: GBW 07601a (Institute of Geophysical and Geochemical Exploration, Langfang, China) and ERM DB001 (Institute for Reference Materials and Measurements, Geel, Belgium). These CRMs were selected because they are comprised of hair, a keratinized tissue similar to horn. Pellets were prepared using a Carver pellet press (Wabash, IN) without the use of a binder.

2.3. Instrumentation and operating conditions

All SR-μXRF analyses were carried out at the Cornell High Energy Synchrotron Source (CHESS), F3 beamline. The F3 beamline station uses a hard bend magnet source. The radiation came from the 5.3 GeV positrons, 21.6 m upstream from the sample. A pair of multilayers with bandpass around 0.6% was used, providing higher monochromatic X-ray flux (˜3 × 10^{10} photons/s) than the standard double-crystal Si(111) monochromator. A CHESS single-bounce mono-capillary was used to generate a 20-μm full width at half maximum (FWHM) focused X-ray beam on the sample. An excitation energy of 16.2 keV was used, and X-ray fluorescence spectra were recorded using a 4-element Vortex silicon-drift detector (SDD) positioned 90 degrees to incident X-rays and with a distance of 22 mm to the sample. An Xspress 3 multichannel analyzer was used for fast data readout and a high fluorescence counting rate. Incident intensity was monitored by an ion chamber upstream of the sample. Samples were analyzed at room temperature in air. Each thin sample was positioned at an angle of 45 degrees from the incident beam and 45 degrees from the detector. A video camera was used to identify the areas to be scanned. 2D raster-mapping in fly-scan mode with dwell times between 0.15 and 0.35 s and step sizes from 35 to 50 μm was performed (Table 1). Shorter dwell times and larger step
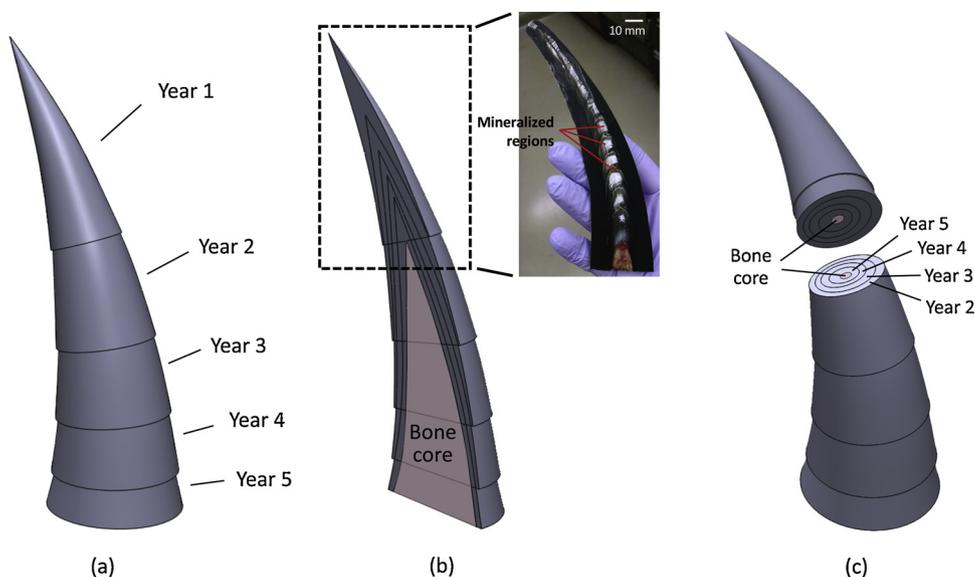
Fig. 1. Growth pattern of caprine horn and location of sample cuts. (a) Diagram of outside of the horn for a hypothetical 5-year old goat indicating the layer of horn grown at each year of age. (b) Diagram of the median sagittal horn section from (a) showing year growth layers in a pattern of stacked cones. Inset of a median sagittal section of the tip of a caprine horn (not analyzed in this study) showing mineralized regions in between year growth layers. (c) Example of a horn cross section, indicating the layer of horn grown at each year of age.

sizes were used for the analysis of CRM pellets. An XRF spectrum was recorded at each analyzed spot for all horn and pellet samples.

2.4. Data analysis

SR-μXRF data were processed using Praxes software, an open source package developed at CHESS (available at https://github.com/praxes/praxes), which uses PyMca libraries for quantitative analysis [27]. Elemental content, calculated as the mass fraction using the fundamental parameters method, was based on an approximation of keratinized matrix composition (chemical formula $C_8H_{14}N_2O_3$) and an average measured horn density of 1.55 g/cm.[3] Sulfur was excluded from the chemical formula due to its low matrix content (~3% by mass) relative to major elements such as carbon. K-shell X-ray lines were used to quantify all elements of interest except Pb, for which the L-lines were used. Elemental images of S were overlaid on Ca using MATLAB and Image Processing Toolbox Release 2017a (The MathWorks, Inc. Natick, Massachusetts, USA) thereby creating composite color images of Ca (green) and S (red).

For validation of quantitative results using CRM pellets, average values were obtained from a representative region of each pellet scan (the largest square area on the circular sample). Uncertainty (u) in the mass fraction estimates shown for the CRMs in Table 2 were calculated based on the ratio of the PyMca reported fitting error (σ area) to the fitted radiation intensity (fit area) for the XRF spectrum peaks of each element of interest, as reported in Praxes for a spectrum averaged over the representative region. The ratio was multiplied by the measured mass fraction for the same area and by 2.355 to obtain the FWHM, or u:

$$u = 2.355 * \left(\frac{\sigma\ area}{fit\ area} \right) * Mass\ fraction \tag{1}$$

For each elemental image of horn cross section samples, several rectangular "regions of interest" (ROI) were identified using Praxes. The width selected for each ROI depended on the radial curvature of Pb

Table 2

Validation of quantitative results using pelletized hair reference materials, ERM DB001 and GBW 07601a.

	ERM DB001		GBW 07601a	
	Found (μg/g)	Certified Value (μg/g)[*]	Found (μg/g)	Certified Value (μg/g)[*]
S	48860 ± 2	–	38500 ± 2300	41900 ± 1100
Ca	992 ± 4	–	1300 ± 90	1450 ± 200
Cu	31 ± 2	33 ± 4	11.4 ± 1.5	14.3 ± 1.6
Zn	255 ± 4	209 ± 12	164 ± 3	137 ± 9
Se	3.2 ± 0.5	3.24 ± 0.24	0.6 ± 0.4	0.58 ± 0.12
Br	7.3 ± 3.3	–	1.7 ± 0.4	(1.1)
Pb	1.8 ± 1.1	2.14 ± 0.20	6.7 ± 1.4	5.7 ± 0.5

(Proposed value)

* Uncertainty provided on Certificate of Analysis.

growth rings and varied from 16 pixels to 57 pixels. The elemental data for each ROI were extracted into Microsoft® Excel (version 16.15 for Mac OS X) and graphed in GraphPad Prism version 7.0e for Mac OS X (GraphPad Software, La Jolla California USA) to depict the Pb mass fraction variation throughout the ROI. Dates were associated with data points within the ROIs by estimating years of formation for each horn growth ring (described in subsection 3.4) and distributing Pb content data within each year evenly over 365 or 366 days. Cross correlation analysis, following resampling of the mass fraction data in order to equalize the number and spacing of points in the two series, was conducted for two samples to explore a possible match between the dosing and Pb deposition using MATLAB and Signal Processing Toolbox Release 2017a. Pearson correlation analyses between elements detected with adequate intensity and exhibiting periodic ring patterns (Ca, S, Zn, Cu, and Br) were carried out using Microsoft Excel and GraphPad Prism. All mass fraction data, excluding the elevated edge data, within each ROI of each sample, were included in the correlation analyses.

Table 1

SR-μXRF scan parameters used for four horn samples and two hair CRM pellets.

	s2001-5sm	s2001-5	s1982-5	s2002-1	CRM Pellets
Dwell time (s)	0.35	0.3	0.35	0.3	0.15
Step size (μm)	40	40	35	40	50
Approx. sample thickness (μm)	230	350	430	250	1650 (ERM DB001), 1300 (GBW 07,601)
Scan square area (mm)	10.80 × 18.40	16.00 × 21.00	15.19 × 11.80	12.00 × 17.60	15.00 × 7.00

3. Results and discussion

3.1. Validation of quantitative results

Validation of quantitative results was performed using two CRMs with certified values for S, Ca, Cu, Zn, Se, Br, and Pb (Table 2). Relative biases were less than 25% for all analytes of interest in this study except Br in GBW 07601a, for which only a "proposed" value is given on the certificate of analysis, indicating a lower confidence than a certified value. For ERM DB001, the found Pb value reported by Praxes software (1.8 ± 1.1 µg/g) is clearly close to the limit of detection (LOD) as reflected by the high relative uncertainty (± 60%) but it is still reasonably close to the certified value of 2.14 ± 0.20 µg/g. LODs for Pb were calculated using areas within ROIs of both samples (s2002-1 and s2001-5) which do not contain any Pb peaks. Within those areas, standard deviations of 10 contiguous points in a line across each ROI were calculated and multiplied by 3 to give an estimated LOD of 1 µg/g for s2001-5 and 1.5 µg/g for s2002-1. Differences in sample thickness and/or biological variability likely explain the difference in LODs for the two samples, which were derived from two different animals. The estimated LODs are indicated in Fig. 6 as red lines to help delineate the Pb signal from background.

3.2. Pb, Ca, S distribution in horn cross sections

Elemental maps produced from SR-µXRF analysis of horn cross-sections show a series of discrete, narrow Pb bands hereafter referred to as "rings" (Fig. 2). Multiple Pb rings were observed in all horn cross-sections examined. The strong Pb signal observed at the surface edges is discussed in subsection 3.6. A crack is visible in the lower region of sample s2001-5 and sections of the outer surface are missing in s2002-1 and s1982-5, probably as a result of mechanical abrasion during the animals' lifetimes (Fig. 2). Fig. 2 shows elemental maps for Pb, Ca, and S for s2001-5 (Fig. 2a), s2002-1 (Fig. 2b), and s1982-5 (Fig. 2c) respectively. Representative XRF point spectra from s2002-1 show a S-K_α peak in a region with a higher S signal relative to Ca (Fig. 3a), in contrast to a nearby region with a diminished S signal relative to Ca (Fig. 3b). Due to the smaller number of distinct Pb rings apparent in the elemental map for s1982-5 compared to s2001-5 and s2002-1, further analysis of the data to link these Pb rings with Pb dosing history was carried out but only for the latter two samples.

3.3. Horn growth pattern

The "nested cones" model of horn growth, described previously, states that the newest "cones" of horn form against the bony core, pushing previously formed cones outward and upward towards the horn tip (Fig. 1) [28]. The central voids observed in all samples except s1982-5 correspond to the vacated position of the most recently formed horn cone in each cross section (Fig. 2). Consistent with this pattern, samples s2002-1 and s2001-5 do not include growth from the last year (s) of animal life (Fig. 4). In contrast to trees, otoliths, and many other incremental growth materials, new layers of horn are formed internally. Therefore, for a given cross section of horn, only the first, outermost layer that is formed has been exposed to the environment and is subject to exogenous contamination. This results in a lower overall contribution from exogenous deposition in horns compared to, for example, a high-surface area keratinized tissue such as hair. Keratinized tissue layers are metabolically inert once formed [29], making transfer of elemental contents between growth layers unlikely. By contrast, tree sapwood, which contains "living" layers, may be able to translocate elemental contents [12].

3.4. Establishment of a horn growth timeline

Elemental images of horn cross sections (Fig. 2) show Ca accumulations in repeating thin bands in each sample, and strong Ca accumulations co-located with white deposits in the bony center or on the boundary of the bone cavity. Longitudinal horn sections also reveal repeating white deposits (Fig. 1b). This suggests that these horns contain alternating regions of primarily keratinized and primarily mineralized regions: the former regions are enriched in S, likely from cysteine's sulfhydryl groups, and the latter are enriched in Ca.

The detection of regions of mineralization located in between the keratinized layers of animal horn was reported previously [30–32]. Using X-ray diffraction and transmission electron microscopy, Hashiguchi, Hashimoto, and Akao observed mineralized regions in between layers of keratinized tissue in horns from the serow [30] and saiga [31], two ruminant species related to goats. The authors suggested that the crystalline inorganic component in both horns contains Ca in the form of octacalcium phosphate (OCP). A later study of rhinoceros horn by Hieronymus et al. (2006) noted periodic regions which the authors hypothesized contained OCP [32]. Hashiguchi & Hashimoto (1995) and Hieronymous et al. both noted that the areas of mineralized tissue varied with annual periodicity, independent of environment. Hashiguchi and Hashimoto (1995) further suggested that increments of horn growth are formed by alternating periods of rapid horn growth and rest that are related to the animal's "biological clock" [30].

Seasonal variation in horn growth rate has been investigated in several studies. An annual slowing or arrest in horn [6,33–37] and overall body growth during the breeding season has been found for many ruminants, including domestic, wild, and castrated animals [38]. Local photoperiod and climatic factors influence breeding season timing; in ruminants, including goats, the breeding season typically falls in Autumn or Winter [38]. Horn annuli – horizontal grooves in the horn surface that form by the end of each winter – have long been used in hunting and wildlife-related research to estimate animal age [36]. The reliability of age determination in certain species using the "horn annulus technique" was established in a study that reported good agreement between horn segment counts and the known ages for 21 bighorn rams [36]. The dating technique was further evaluated in subsequent studies including other ruminant species [37,39,40].

Based on the distinct Ca rings and white deposits observed here in caprine horns, we suggest that during the annual breeding period each autumn, keratin deposition is temporarily arrested to form an "annulus," and a layer of mineralized tissue is deposited. These mineralized regions can be identified by their enriched Ca content. Using the distinct pattern of Ca accumulations observed in horn cross sections, an estimated year of formation can be assigned to each layer to create a "timeline" of horn growth. Dates begin with the earliest-formed (outer) layer of horn, based on the longitudinal position of the original sample cuts. Consistent with previous studies [35], the first year's annulus is the least defined for the horns 2001-5 and 2002-1 in this study, both along the outside of the horn and within cross sections. Therefore, the best date estimates used here have an uncertainty of ± 1 year. Future studies could increase confidence in the absolute dates assigned by using cross sections that include the bony core, such that the innermost horn layer corresponds to the final year of life. Horn growth timelines for s2001-5 and s2002-1 are shown in Fig. 4.

By extrapolating conception dates from birthdates of 46 goats, we were able to estimate the timing window of the breeding season for the specific caprine herd investigated in this study. Similar to many ruminants, the breeding season for this population is estimated to occur in Autumn, with most conceptions occurring in the second half of October. The precise timing and duration of horn annuli formation is not known, however, and it can only be assumed to take place by the end of Winter [36]. Annual breakpoint estimates are assigned as January 1 in the horn growth timelines. An additional uncertainty of ~3 months is associated with these estimates, considering that the actual timing of horn growth arrest may fall anytime between early Autumn and late Winter (Fig. 4). Further studies using confocal XRF and XRD mapping may be able to
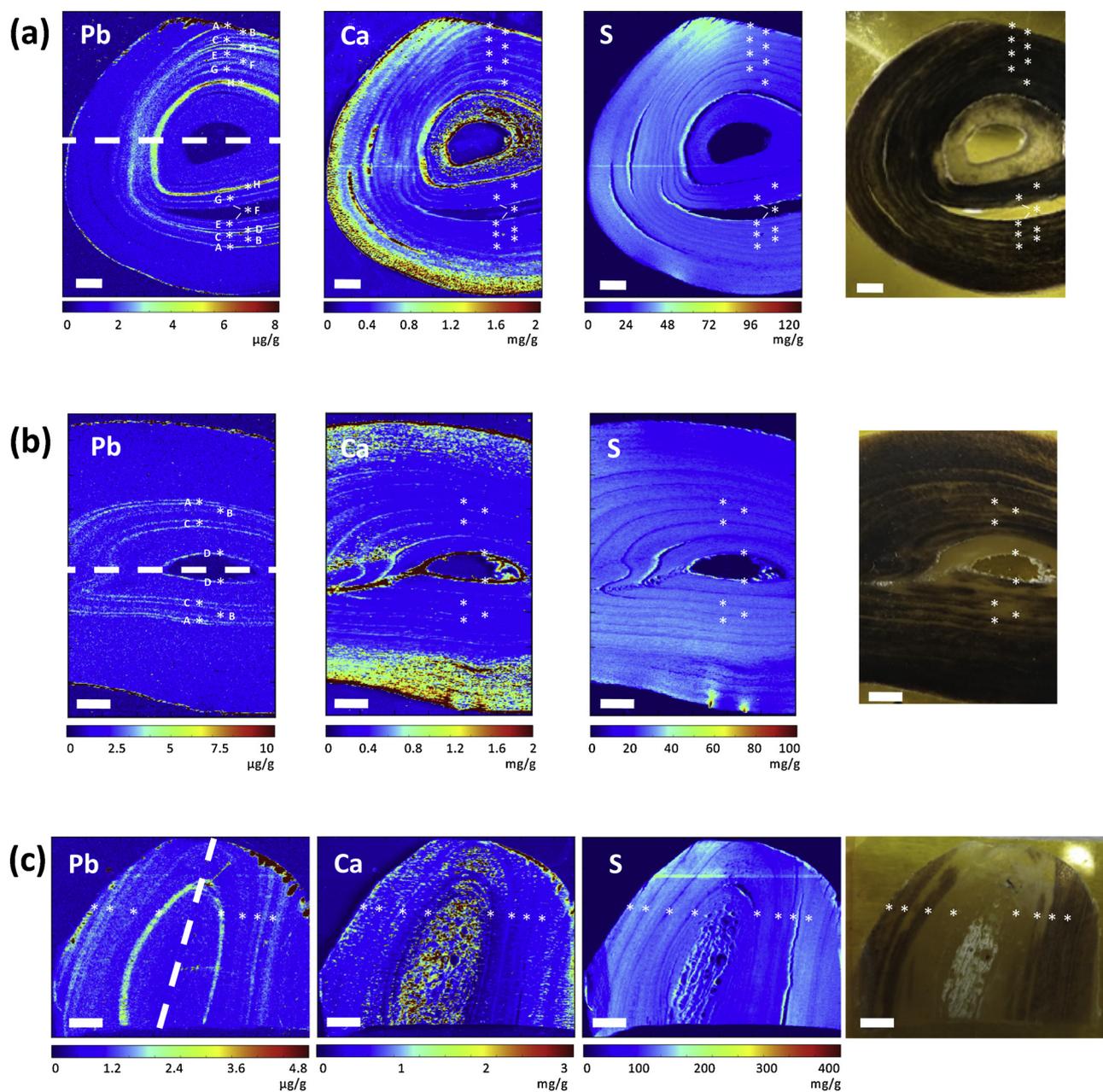
Fig. 2. Digital images and quantitative Pb (µg/g), Ca (mg/g), and S (mg/g) µXRF maps of a horn cross section from goat (a) 2001-5, (b) 2002-1, and (c) 1982-5. Asterisks denote discrete Pb rings or pairs of rings at the estimated boundaries between horn growth layers, labeled in s2001-5 (A–H) and s2002-1 (A–D). Dashed line indicates an approximate axis of symmetry of Pb rings. Scale bar = 2 mm.

verify mineralization between keratin rings.

3.5. Investigating the relationship between historical Pb dosing and the varying spatial Pb distribution across horn cross sections

Timelines of horn growth described in section 3.4 were superimposed on Pb elemental images for samples s2001-5 and s2002-1 (Fig. 5). Visual inspection of Fig. 5 suggests that the Pb content varies from one ring to the next within each ROI. The dosing regimen used to produce the blood Pb PT pools was also variable. Therefore, we investigated the relationship between the spatial Pb distribution and the historical dosing schedules for samples derived from two different animals.

Pb data were extracted from Praxes software and graphed as a line scan, with each data point representing the average of 16 to 57 contiguous pixels selected from within each ROI (Fig. 4,5). Each data point

in the line scans shown in Fig. 6 was assigned an estimated date (mm/dd/yyyy) based on the annual breakpoints determined from the horn growth timelines for each animal (s2001-5 and s2002-1), assuming a simplified constant within-year growth. A Pb line scan corresponding to each ROI was then graphed on the same x-axis as the dosing time series, with the breakpoint of January 1 of each year indicated (Fig. 6).

For both animals, the first recorded oral Pb dose is followed by a distinct Pb peak(s), as observed in Fig. 6, suggesting a time lag between Pb ingestion and deposition in horn. By visually examining the time between the first dose and the first Pb peak in Fig. 5, we can estimate this time lag as approximately one year for both animals. However, as discussed in subsection 3.4, the actual date of Pb deposition is subject to considerable uncertainty. We used cross correlation analysis as a secondary approach to explore the temporal relationship between time of dosing and Pb deposition in these horn samples. Cross correlation can be used to assess the similarity between 2 time series at various relative
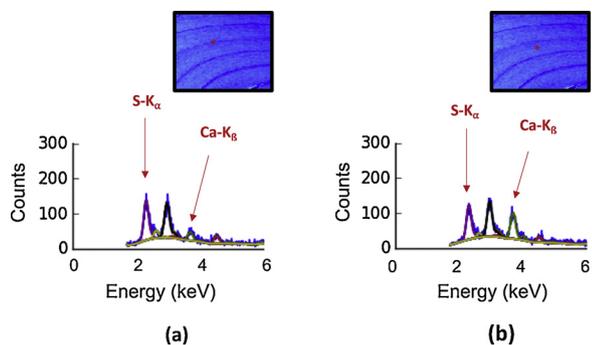
Fig. 3. Examples of XRF point spectra from (a) a keratinized zone, enriched in S, and (b) a mineralized zone, enriched in Ca for s2002-1. Insets show the µXRF maps for S, with asterisks indicating approximately where the point spectra were obtained.

lags and has been employed in chronology studies of trees and lichens [41,42], marine tissues [41,43], and other materials [44]. The approach can also be used to estimate the time lag between 2 series. In this study, cross correlation coefficients at the optimum lag, on a scale of 0 (no correlation) to 1 (perfect correlation), were calculated as 0.16 for s2001-5 and 0.11 for s2002-1, indicating weak correlations for both ROIs of both samples. The correlation coefficients for both ROIs of s2002-1 were particularly weak, and no single optimum lag was identified by the cross correlation. As mentioned, a time lag of about 1 year between Pb dosing and Pb deposition in s2002-1 can be estimated visually from Fig. 6b. For s2001-5, based on cross correlation calculations for both ROIs, the transfer of Pb from date of dose to deposition was estimated to lag dosing by ~347 to 383 days, which is consistent with visual observations in Fig. 6. The uncertainty in assigning a precise date to each of the horn growth rings, coupled with Pb XRF data that are close to the LOD, presents a particular challenge when calculating these time lag estimates.

The weak cross correlations between the Pb distribution and dosing history in these samples suggests that Pb uptake into these horns may
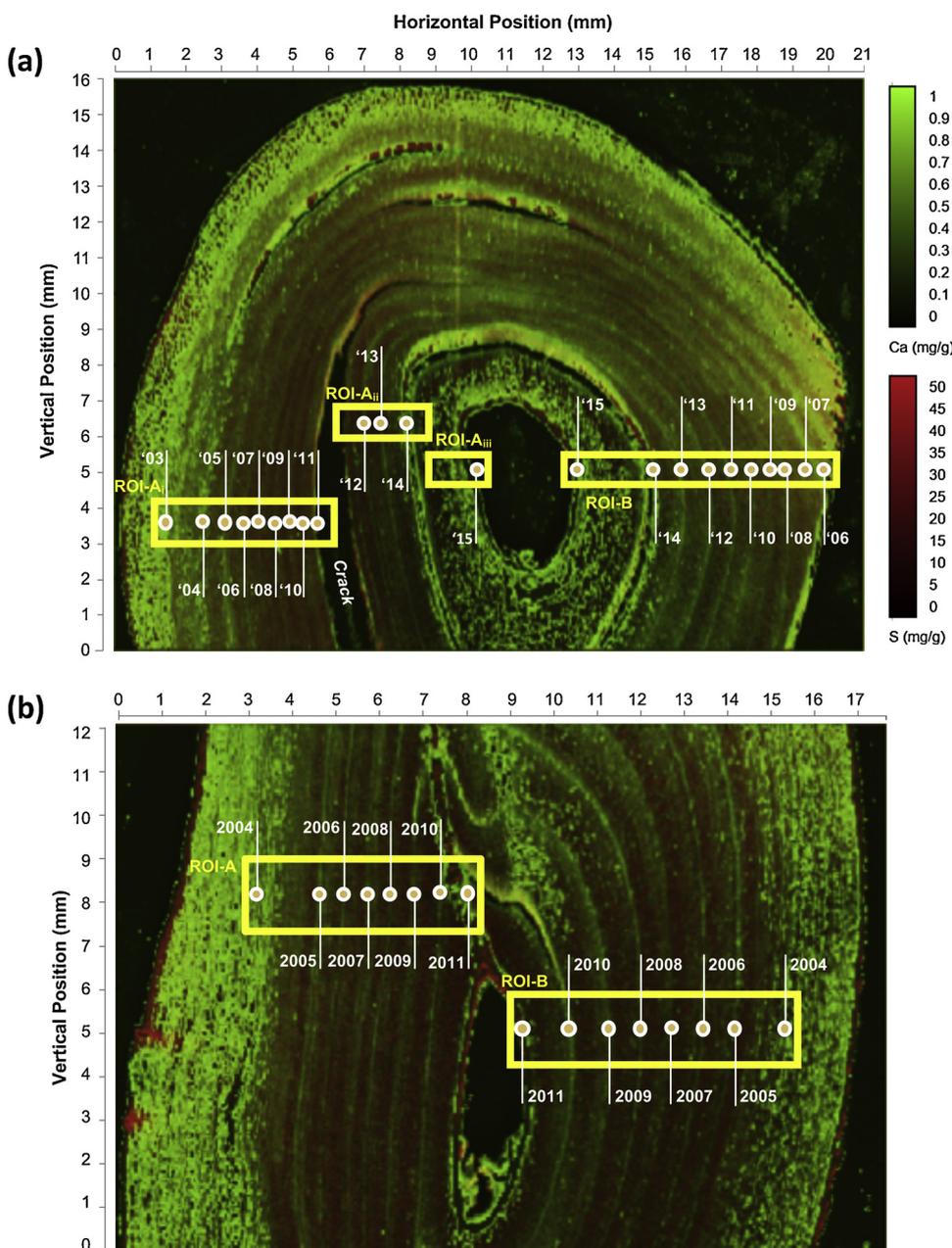

Fig. 4. Horn growth timelines superimposed on composite images of Ca (green) and S (red) µXRF maps for (a) s2001-5 and (b) s2002-1. Annual horn growth layers (denoted by 📍) are labeled within symmetrical ROI-A and ROI-B in both images, beginning with the oldest growth on the outside. Extreme Ca values on the sample edges (> 1 mg/g) are excluded to enhance details at lower Ca levels. Both maps are rotated 90 degrees clockwise relative to Fig. 2a, b. Years are denoted by the last two digits in (a), e.g., '01 means 2001.
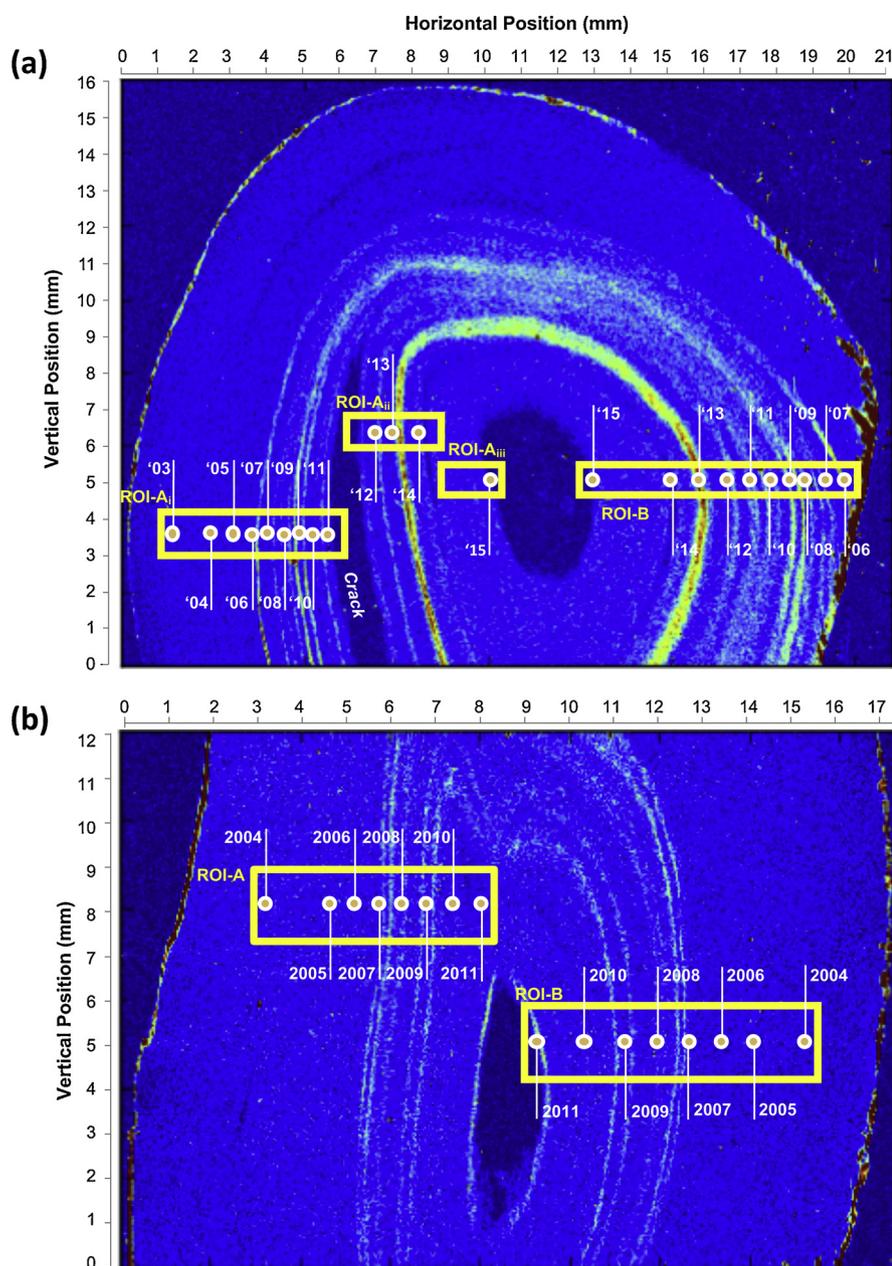
Fig. 5. Horn growth timelines superimposed on Pb µXRF maps for (a) s2001-5 and (b) s2002-1. Annual horn growth layers (denoted by 📍) are labeled within symmetrical ROI-A and ROI-B in both images, beginning with the oldest growth on the outside. Both maps are rotated 90 degrees clockwise relative to Fig. 2a, b. Years are denoted by the last two digits in (a), e.g., '01 means 2001.

reflect complex recycling of Pb between body compartments after multiple Pb doses. It is well known that Pb accumulates in the bone compartment and can re-mobilize into the blood in response to physiological changes (e.g., during pregnancy). In ruminants, the gastrointestinal system is more complex, which likely plays an additional role in Pb absorption and recycling but the exact mechanism is unclear [15]. Another possibility is that the Pb distribution may reflect the specific mechanism of horn growth; for example, Pb rings may be deposited within the mineralized regions of horn following Ca deposition. Accumulation of Pb in mineralized horn regions would not be surprising: physiologically, Pb mimics Ca and accumulates in mineralized tissues such as bone, including goat bone [23]. However, the existence of Pb rings that are narrower than the lateral spatial resolution of the XRF setup used in this study, and hence the possibility that Pb is deposited into horn continuously, cannot be ruled out. In a similar case of Hg deposition in hair, for example, Hg accumulations have been shown to be resolvable at small time scales as short as one day [45]. Further investigation of Pb distributions in horn cross sections at higher spatial resolution could answer remaining questions about the mechanism of Pb uptake into horn.

3.6. Elevated edge signals for Pb and other elements

An intense Pb X-ray signal is observed at the outer surface of these horn samples. Zinc and Ca also show elevated edge signals. The X-ray spectral fit for a representative region near the upper edge of s2002-1 confirms these signals are based on true peaks in that region, rather than artifacts of analyzing at the edge of the sample (Fig. 7).

The surface of the horn cross-section samples examined here represents growth from the early years of life when animals were not dosed with Pb. All keratinized tissues are exposed to the outside environment and are potentially subject to surface contamination. Distinguishing between exogenous and endogenous content is challenging, especially for tissues that have a high surface to volume ratio (e.g., hair and feathers) as well as for elements that are ubiquitous in the environment, such as Pb. Many studies measuring Pb in hair have reported exogenous deposition, as indicated by an increase in Pb content along the hair shaft [16,46–52]. The surface of the horn cross-section
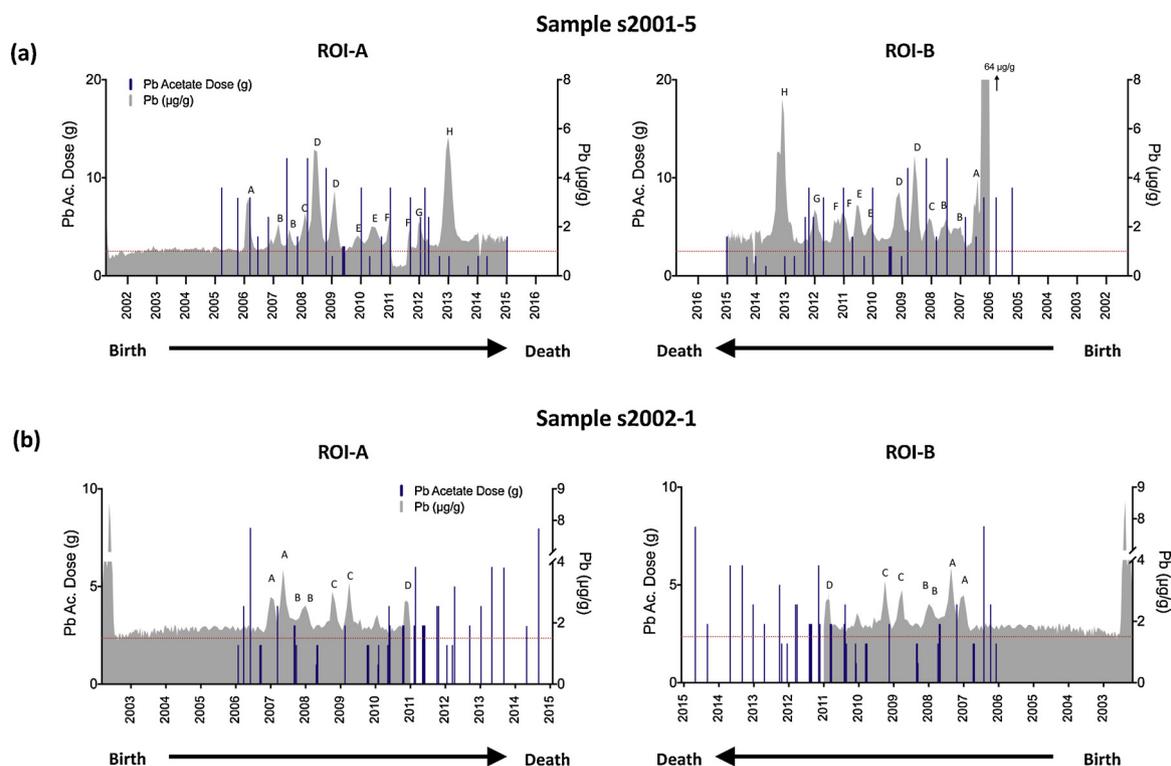
Fig. 6. Variation in Pb content matched to the horn growth timeline and to the historical Pb acetate dose schedule for sample (a) s2001-5 and (b) s2002-1. SR-µXRF averaged line scan (gray) showing Pb mass fraction plotted as a function of time using dates from the horn growth timelines in Fig. 4 along the symmetrical left (ROI-A) and right (ROI-B) halves of each sample. Pb peaks corresponding to rings in Fig. 2 are labeled in s2001-5 (A–H) and s2002-1 (A–D). The lifelong dosing timeline for the animal (navy), with bars corresponding to the cumulative Pb acetate dose over dosing events of up to 7 days, is overlaid on the line scan. Estimated LODs are indicated by red dotted lines. Annual breakpoints represent January 1 of the listed year.
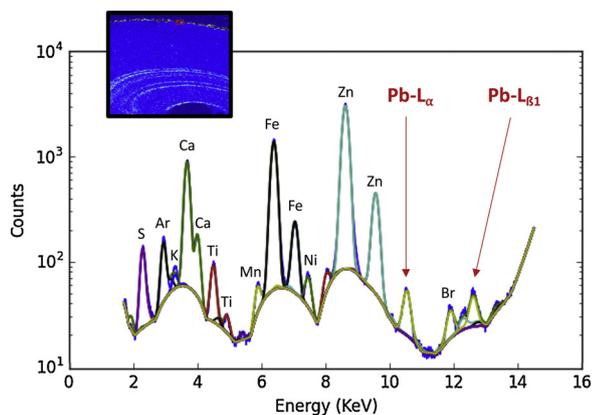

Fig. 7. X-ray spectrum for the edge region of s2002-1 confirming presence of Pb. Spectra were summed over a ˜0.2 x 0.1 mm rectangle indicated by the red box at upper edge the of the µXRF map inset.

samples examined here represents growth from the early years of life when animals were not dosed with Pb. Thus, the Pb deposition observed on the outer horn surface in this study is most likely due to external contamination rather than endogenous excretion. In horns, the high relative volume and new layers that form internally mean that Pb content below the surface is largely unaffected by surface deposition [53].

Elevated Ca and Zn content on the edges of these samples are also likely due to contamination, or to unknown physiological events.

3.7. Additional elements: Se, Cu, Zn, Br

Regions showing Se accumulation appear as diffuse bands rather

than discrete rings, coinciding with the region containing Pb rings (Fig. 8). These patterns could suggest a period of Se enrichment following an acute Pb dosing event, although due to the low resolution of the Se maps, a simple co-location of Se and S in the samples cannot be ruled out. It should be noted that while the XRF peaks for Se-Kβ at 12.5 keV and Pb-Lβ at 12.6 keV overlap in energy dispersive spectrometry, the Se-Kα peak at 11.2 keV and the Pb-Lα peak at 10.5 keV are well resolved (see the Supplementary Figure). Increasing the lateral spatial resolution to image Se accumulation bands might be achieved by higher X-ray flux and longer dwell times, confocal XRF techniques [54], plan-view scanning (rather than 45 degrees), and/or LA-ICP-MS analysis. Previous studies have suggested an antagonistic relationship between Pb and Se in the body [55]. For example, Se may have a protective effect against Pb toxicity, and urinary Se excretion decreases with elevated Pb uptake in cows [56]. There is a possibility that Se incorporation into caprine horns may be affected by Pb uptake based on the elemental imaging reported here. Further spatial analysis with better Se resolution would be necessary to address this question.

Elemental images for Cu and Zn in all three horn cross sections appear to show growth rings similar to those seen for S (Fig. 8). Cu and Zn, like S, have known roles in keratin formation. In its RS- coordination, Zn binds sulfhydryl groups to help form disulfide cross-links in keratin [57]. A close examination of Figs. 2 and 8 show Zn is not consistently co-located with S in these samples: significant Pearson correlations with S were found only for two of the four ROIs investigated, one positive and one negative: s2001-5 ROI-B (r = -0.35) and s2002-1 ROI-A (r = 0.46). Similar to Zn, Cu aids in catalytic oxidation of sulfhydryl groups to disulfides [58,59]. Correlations between Cu and S data were slightly stronger compared to Zn, with moderate to significant correlations found for all four ROIs: s2001-5 ROI-A (r = 0.28), s2001-5 ROI-B (r = 0.33), s2002-1 ROI-A (r = 0.21) and s2002-1 ROI-B (r = 0.35).
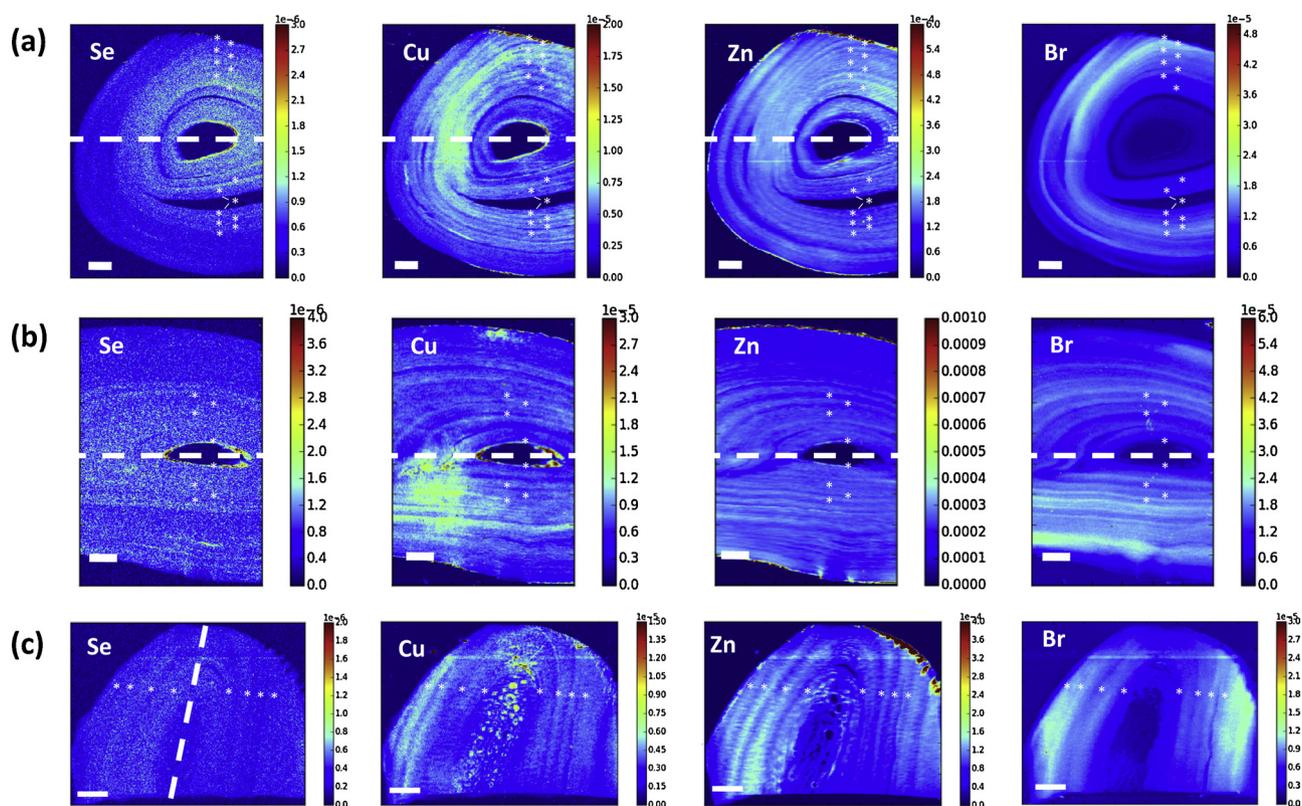
Fig. 8. SR-μXRF elemental maps showing Se (μg/g), Cu (μg/g), Zn (μg/g), and Br (μg/g) distributions in samples (a) s2001-5, (b) s2002-1, and (c) s1982-5. Asterisks denote the exact locations of discrete Pb rings shown in Fig. 3. Dashed line in Se image indicates an approximate axis of symmetry of Pb rings. Scale bar = 2 mm.

Elemental images also reveal distinct, repeating layers of Br accumulation in s2001-5, s2002-1, and s1982-5 (Fig. 8). Consistent with the apparent co-location of Br and S as seen in Figs. 2 and 8, highly significant Pearson correlations were found between Br and S data in these cross-sectional samples: coefficients for ROI-A and ROI-B of s2001-5 and s2002-1 are 0.80, 0.77, 0.62, and 0.52, respectively.

While Br was recently reported to have an essential function in the formation of collagen in Drosophila [60], it has no known role in keratin formation, unlike S, Cu, and Zn. A previous study found that Br-deficient diets led to decreased Br concentrations of skin and hair in rats, suggesting that Br is taken up into keratinized tissues [61]. We thus assume that Br is excreted into horns of the goats in this study following exposure from salt licks, feed, and/or grain. Further investigation is needed to explain the strong co-location of Br with S in these horn samples, compared with more modest correlations found between S, Zn, and Cu; both the latter have known roles in keratin formation.

4. Conclusions

This study provides new information on the relationship between acute Pb exposures and its eventual excretion into caprine horns based on SR-μXRF maps of Pb micro-distributions in horn cross sections. These data suggest that, in response to ingestion exposure, Pb is taken up into caprine horns, resulting in discrete accumulations. Localized enrichment of Cu, Zn, Br and S appear to coincide with the keratinized regions related to the annual growth ring pattern in horns. A marginal increase in Se may coincide with Pb accumulation in horn cross-sections. Variation in Ca-rich layers with annual periodicity in caprine horn cross-sections is evident, consistent with previous reports of horn mineralization. A growth timeline for each horn cross section was established based on the alternating mineralization (Ca bands) and keratinized (S bands) regions. The timelines were used to link dosing events with the eventual deposition of Pb in the horn samples studied.

While the data suggest that Pb deposition in horns occurs during the dosing time period, the spatial distribution is not an exact match with the temporal dosing regimen. Spatial analysis of horns for Pb accumulation may be useful as a qualitative marker of time-resolved exposures that may reflect specific periods of acute Pb absorption.

Acknowledgments

Appendix A. Supplementary data

Supplementary material related to this article can be found, in the online version, at doi:https://doi.org/10.1016/j.jtemb.2019.05.013.

References

[1] K.R. Mahaffey, G.E. Rice, Mercury Study Report to Congress. Volume 4. An Assessment of Exposure to Mercury in the United States, (1996) http://www.osti.gov/energycitations/product.biblio.jsp?osti_id=285172%5Cnpapers2://publication/uuid/EFE94F34-17C0-4040-8317-7BDE93B5961A.
[2] A. Neville, Daily growth layers in animals and plants, Biol. Rev. 42 (1967) 421–441.
[3] M.D. Seltzer, K.H. Berry, Laser ablation ICP-MS profiling and semiquantitative determination of trace element concentrations in desert tortoise shells: documenting the uptake of elemental toxicants, Sci. Total Environ. 339 (2005) 253–265, https://doi.org/10.1016/j.scitotenv.2004.07.027.
[4] M.C. Dean, Growth layers and incremental markings in hard tissues; a review of the literature and some preliminary observations about enamel structure in Paranthropus boisei, J. Hum. Evol. 16 (1987) 157–172, https://doi.org/10.1016/0047-2484(87)90074-1.
[5] G. Caumette, S. Ouypornkochagorn, C.M. Scrimgeour, A. Raab, J. Feldmann, Monitoring the arsenic and iodine exposure of seaweed-eating North Ronaldsay sheep from the gestational and suckling periods to adulthood by using horns as a dietary archive, Environ. Sci. Technol. 41 (2007) 2673–2679.
[6] P. Iacumin, H. Bocherens, L. Chaix, Keratin C and N stable isotope ratios of fossil

cattle horn from Kerma (Sudan): a record of dietary changes, Ital. J. Quat. Sci. 14 (2001) 41–46.

[7] I. Barbosa, M. Kley, R. Schaufele, K. Auerswald, W. Schroder, F. Filli, S. Hertwig, H. Schnyder, Analysing the isotopic life history of the alpine ungulates Capra ibex and Rupicapra rupicapra rupicapra through their horns, Rapid Commun, Mass Spectrom. 23 (2009) 2347–2356, https://doi.org/10.1002/rcm.

[8] I. Barbosa, I.H. Köhler, K. Auerswald, P. LüPs, H. Schnyder, Last-century changes of alpine grassland water-use efficiency: a reconstruction through carbon isotope analysis of a time-series of Capra ibex horns, Glob. Chang. Biol. 16 (2010) 1171–1180, https://doi.org/10.1111/j.1365-2486.2009.02018.x.

[9] K.T. Uno, J. Quade, D.C. Fisher, G. Wittemyer, I. Douglas-Hamilton, S. Andanje, P. Omondi, M. Litoroh, T.E. Cerling, Bomb-curve radiocarbon measurement of recent biologic tissues and applications to wildlife forensics and stable isotope (paleo) ecology, Proc. Natl. Acad. Sci. 110 (2013) 11736–11741, https://doi.org/10.1073/pnas.1302226110.

[10] A.E. Kelly, M.K. Reuer, N.F. Goodkin, E.A. Boyle, Lead concentrations and isotopes in corals and water near Bermuda, 1780-2000, Earth Planet. Sci. Lett 283 (2009) 93–100, https://doi.org/10.1016/j.epsl.2009.03.045.

[11] K. Spencer, D.J. Shafer, R.W. Gauldie, E.H. DeCarlo, Stable lead isotope ratios from distinct anthropogenic sources in fish otoliths: a potential nursery ground stock marker, Comp. Biochem. Physiol. - A Mol. Integr. Physiol. 127 (2000) 273–284, https://doi.org/10.1016/S1095-6433(00)00260-9.

[12] S.A. Watmough, Monitoring historical changes in soil and atmospheric trace metal levels by dendrochemical analysis, Environ. Pollut. 106 (1999) 391–403, https://doi.org/10.1016/S0269-7491(99)00102-5.

[13] B. Vermillion, R. Brugam, L. Retzlaff, I. Bala, The sedimentary record of environmental lead contamination at St. Louis, Missouri (USA) area smelters, J. Paleolimnol. 33 (2005) 189–203, https://doi.org/10.1007/s10933-004-4078-x.

[14] M.C. Newman, M. Mulvey, A. Beeby, R.W. Hurst, L. Richmond, Snail (Helix aspersa) exposure history and possible adaptation to lead as reflected in shell composition, Arch. Environ. Contam. Toxicol. 27 (1994) 346–351, https://doi.org/10.1007/BF00213170.

[15] F. Barbosa, J.E. Tanus-Santos, R.F. Gerlach, P.J. Parsons, A critical review of bio-markers used for monitoring human exposure to lead: advantages, limitations, and future needs, Environ. Health Perspect. 113 (2005) 1669–1674, https://doi.org/10.1289/ehp.7917.

[16] H. Skröder, M. Kippler, B. Nermell, F. Tofail, M. Levi, S.M. Rahman, R. Raqib, M. Vahter, Major Limitations in Using Element Concentrations in Hair as Biomarkers of Exposure to Toxic and Essential Trace Elements in Children, Environ. Health Perspect. 125 (2017) 1–9, https://doi.org/10.1289/EHP1239.

[17] E. Esteban, C.H. Rubin, R.L. Jones, G. Noonan, Hair and blood as substrates for screening children for lead poisoning, Arch. Environ. Health 54 (1999) 436–440, https://doi.org/10.1080/00039899909603376.

[18] B.L. Gulson, Nails: concern over their use in lead exposure assessment, Sci. Total Environ. 177 (1996) 323–327, https://doi.org/10.1016/0048-9697(95)04896-0.

[19] M.B. Rabinowitz, G.W. Wetherill, J.D. Kopple, Kinetic analysis of lead metabolism in healthy humans, J. Clin. Invest. 58 (1976) 260–270, https://doi.org/10.1172/JCI108467.

[20] P. Grandjean, Lead poisoning: hair analysis shows the calendar of events, Hum. Toxicol. 3 (1984) 223–228.

[21] K.E. Murphy, W.F. Guthrie, T.W. Vetter, G.C. Turk, C.D. Palmer, J.M.E. Lewis, C.M. Geraghty, P.J. Parsons, Comparison of clinical methods with isotope dilution inductively coupled plasma mass spectrometry for the new standard reference material 955c lead in caprine blood, J. Anal. At. Spectrom. 24 (2009) 1170–1178, https://doi.org/10.1039/B903060C.

[22] P.J. Parsons, Monitoring human exposure to lead: an assessment of current laboratory performance for the determination of blood lead, Environ. Res. 57 (1992) 149–162.

[23] Y. Cretacci, P.J. Parsons, Localized accumulation of lead within and among bones from lead-dosed goats, Environ. Res. 110 (2010) 26–32, https://doi.org/10.1016/j.envres.2009.09.005.

[24] A.J. Steuerwald, F.S. Blaisdell, C.M. Geraghty, P.J. Parsons, Regional distribution and accumulation of lead in caprine brain tissues following a long-term oral dosing regimen, J. Toxicol. Environ. Health. A. 77 (2014) 663–678, https://doi.org/10.1080/15287394.2014.880328.

[25] P.C. Kruger, C.M. Geraghty, P.J. Parsons, Development of caprine liver quality control materials for trace element analysis of biological tissues, Accredit. Qual. Assur. 15 (2010) 451–458, https://doi.org/10.1007/s00769-010-0660-2.

[26] P.J. Parsons, A.A. Reilly, D. Esernio-Jenssen, L.N. Werk, H.C. Mofenson, N.V. Stanton, T.D. Matte, Evaluation of blood lead proficiency testing: comparison of open and blind paradigms, Clin.Chem. 47 (2001) 322–330.

[27] V.A. Solé, E. Papillon, M. Cotte, P. Walter, J. Susini, A multiplatform code for the analysis of energy-dispersive X-ray fluorescence spectra, Spectrochim. Acta - Part B At. Spectrosc. 62 (2007) 63–68, https://doi.org/10.1016/j.sab.2006.12.002.

[28] E.B. Davis, K a Brakora, A.H. Lee, Evolution of ruminant headgear: a review, Proc. Biol. Sci. 278 (2011) 2857–2865, https://doi.org/10.1098/rspb.2011.0938.

[29] A.G, C.P. Leblond, The Keratinization of Epidermis and Its Derivaties, Especially the Hair, As Shown by X-ray Diffraction and Histochemical Studies, (1957), pp. 845–851.

[30] K. Hashiguchi, K. Hashimoto, The mineralization of crystalline inorganic compo-nents in japanese serow horn, Okajimas Folia Anat. 72 (1995) 235–243, https://doi.org/10.2535/ofaj1936.72.5_235.

[31] K. Hashiguchi, K. Hashimoto, M. Akao, Morphological character of crystalline components present in Saiga horn, Okajimas Folia Anat. 78 (2001) 43–48.

[32] T.L. Hieronymus, L.M. Witmer, R.C. Ridgely, Structure of white Rhinoceros (Ceratotherium simum) horn investigated by X-ray computed tomography and

[33] A. Toledano-Díaz, J. Santiago-Moreno, A. Gómez-Brunet, A. Pulido-Pastor, A. López-Sebastián, Horn growth related to testosterone secretion in two wild Mediterranean ruminant species: the Spanish ibex (Capra pyrenaica hispanica) and European mouflon (Ovis orientalis musimon), Anim. Reprod. Sci. 102 (2007) 300–307, https://doi.org/10.1016/j.anireprosci.2006.10.021.

[34] M. Festa-Bianchet, D.W. Coltman, L. Turelli, J.T. Jorgenson, Relative allocation to horn and body growth in bighorn rams varies with resource availability, Behav. Ecol. 15 (2004) 305–312, https://doi.org/10.1093/beheco/arh014.

[35] T.J. McDonough, J.R. Crye, G.G. Del Frate, Can Horn Length of Mountain Goats Be Used as a Measure of Habitat Quality? Bienn. Symp. North. Wild Sheep Goat Counc. 15 (2006) 158–166.

[36] V. Geist, Validity of horn segment counts in aging bighorn sheep, J. Wildl. Manage. 30 (1966) 634–635.

[37] J.E. Hemming, Cemental Deposition, Tooth Succession, and Horn Development as Criteria of Age in Dall Sheep, J. Wildl. Manage. 33 (1969) 552–558.

[38] S.W. Walkden-Brown, Seasonality in male Australian cashmere goats: long term effects of castration and testosterone or oestradiol treatment on changes in LH, FSH and prolactin concentrations, and body growth, Small Rumin. Res. 26 (1997) 239–252, https://doi.org/10.1016/S0921-4488(97)00017-5.

[39] F.L. Bunnell, Horn growth and population quality in dall sheep, J. Wildl. Manage. 42 (1978) 764–775.

[40] V. Stevens, D.B. Houston, Reliability of age determination of mountain goats, Wildl. Soc. Bull. 17 (1989) 72–74.

[41] B.A. Black, D. Griffin, P. van der Sleen, A.D. Wanamaker, J.H. Speer, D.C. Frank, D.W. Stahle, N. Pederson, C.A. Copenheaver, V. Trouet, S. Griffin, B.M. Gillanders, The value of crossdating to retain high-frequency variability, climate signals, and extreme events in environmental proxies, Glob. Chang. Biol. 22 (2016) 2582–2595, https://doi.org/10.1111/gcb.13256.

[42] V. Winchester, S. Harrison, Dendrochronology and lichenometry: colonization, growth rates and dating of geomorphological events on the east side of the North Patagonian Icefield, Chile, Geomorphology 34 (2000) 181–194, https://doi.org/10.1016/S0169-555X(00)00006-4.

[43] L.M. Clarke, K.D. Friedland, Influence of growth and temperature on strontium deposition in the otoliths of Antlantic salmon, J. Fish Biol. 65 (2004) 744–759, https://doi.org/10.1111/j.1095-8649.2004.00480.x.

[44] M. Tan, A. Baker, D. Genty, C. Smith, J. Esper, B. Cai, Applications of stalagmite laminae to paleoclimate reconstructions: comparison with dendrochronology/cli-matology, Quat. Sci. Rev. 25 (2006) 2103–2117, https://doi.org/10.1016/j.quascirev.2006.01.034.

[45] M. Legrand, R. Lam, M. Jensen-Fontaine, E.D. Salin, H. Man Chan, Direct detection of mercury in single human hair strands by laser ablation inductively coupled plasma mass spectrometry (LA-ICP-MS), J. Anal. At. Spectrom. 19 (2004) 1287–1288, https://doi.org/10.1039/b406733a.

[46] M.L. Carvalho, A.F. Marques, J.A.A. Brito, Synchrotron radiation and energy dis-persive X-ray fluorescence applications on elemental distribution in human hair and bones, 19th International Conference on X-Ray and Inner-Shell Processes: American Institute of Physics, (2003), pp. 522–528.

[47] R.R. Martin, I.M. Kempson, S.J. Naftel, W.M. Skinner, Preliminary synchrotron analysis of lead in hair from a lead smelter worker, Chemosphere. 58 (2005) 1385–1390, https://doi.org/10.1016/j.chemosphere.2004.09.087.

[48] A. Baysal, S. Akman, Determination of lead in hair and its segmental analysis by solid sampling electrothermal atomic absorption spectrometry, Spectrochim. Acta - Part B At. Spectrosc. 65 (2010) 340–344, https://doi.org/10.1016/j.sab.2010.02.016.

[49] V.L. Dressler, D. Pozebon, M.F. Mesko, A. Matusch, U. Kumtabtim, B. Wu, J. Sabine Becker, Biomonitoring of essential and toxic metals in single hair using on-line solution-based calibration in laser ablation inductively coupled plasma mass spec-trometry, Talanta. 82 (2010) 1770–1777, https://doi.org/10.1016/j.talanta.2010.07.065.

[50] A.J.J. Bos, C.C.A.H. van der Stap, V. Valković, R.D. Vis, H. Verheul, Incorporation routes of elements into human hair; implications for hair analysis used for mon-itoring, Sci. Total Environ. 42 (1985) 157–169, https://doi.org/10.1016/0048-9697(85)90015-4.

[51] I.M. Kempson, W.M. Skinner, K.P. Kirkbride, Advanced analysis of metal distribu-tions in human hair, Environ. Sci. Technol. 40 (2006) 3423–3428, https://doi.org/10.1021/es052158v.

[52] H.H. Sky-Peck, Distribution of trace elements in human hair, Clin. Physiol. Biochem. 8 (1990) 70–80.

[53] L. Hu, Spatial Concentrations of Trace Elements in Keratin, The University of Utah, 2016.

[54] S. Choudhury, D.N. Agyeman-Budu, A.R. Woll, T. Swanston, T.L. Varney, D.M.L. Cooper, E. Hallin, G.N. George, I.J. Pickering, I. Coulthard, Superior spatial resolution in confocal X-ray techniques using collimating channel array optics: elemental mapping and speciation in archaeological human bone, J. Anal. At. Spectrom. 32 (2017) 527–537, https://doi.org/10.1039/c6ja00297h.

[55] M. Ahamed, M.K.J. Siddiqui, Environmental lead toxicity and nutritional factors, Clin. Nutr. 26 (2007) 400–408, https://doi.org/10.1016/j.clnu.2007.03.010.

[56] M.W. Neathery, W.J. Miller, R.P. Gentry, C.T. Crowe, E. Alfaro, A.S. Fielding, D.G. Pugh, D.M. Blackmon, Influence of high dietary lead on selenium metabolism in dairy calves, J. Dairy Sci. 70 (1987) 645–652, https://doi.org/10.3168/jds.S0022-0302(87)80054-1.

[57] R.J.P. Williams, Zinc: what is its role in biology? Endeavour 8 (1984) 65–70, https://doi.org/10.1016/0160-9327(84)90040-1.

[58] C.-H. Lee, M.-S. Kim, B.M. Chung, D.J. Leahy, P.A. Coulombe, Structural basis for

heteromeric assembly and perinuclear organization of keratin filaments, Nat. Struct. Mol. Biol. 19 (2012) 707–715, https://doi.org/10.1038/nsmb.2330.

[59] R.C. Marshall, D.F.G. Orwin, J.M. Gillespie, Structure and biochemistry of mammalian hard keratin, Electron Microsc. Rev. 4 (1991) 47–83, https://doi.org/10.1680/udap.2010.163.

[60] A.S. McCall, C.F. Cummings, G. Bhave, R. Vanacore, A. Page-McCaw, B.G. Hudson, Bromine is an essential trace element for assembly of collagen IV scaffolds in tissue development and architecture, Cell 157 (2014) 1380–1392, https://doi.org/10.1016/j.jneumeth.2010.08.011.Autogenic.

[61] P.S. Winneck, A.H. Smith, The determination of bromine in biological substances, J. Biol. Chem. 119 (1937) 93–101.